ChemComm

COMMUNICATION

View Article Online
View Journal

Check for updates

Cite this: DOI: 10.1039/c9cc09652c

Received 12th December 2019,
Accepted 28th January 2020

DOI: 10.1039/c9cc09652c

rsc.li/chemcomm

Published on 28 January 2020. Downloaded by Universite Paris Descartes on 2/7/2020 3:20:41 AM.

Observation of peroxynitrite overproduction in cells during 5-fluorouracil treatment *via* a ratiometric fluorescent probe†

Ji-Ting Hou, *[ab] Bingya Wang,[a] Yongru Zhang,[c] Beibei Cui,[a] Xinhua Cao,[a] Man Zhang,[d] Yong Ye *[c] and Shan Wang *[a]

We describe a colorimetric and fluorescent probe 3a to detect cellular peroxynitrite with high selectivity and sensitivity. 3a was successfully applied in the bioimaging of exogenous and endogenous peroxynitrite in living cells. The up-regulation of peroxynitrite in cancer cells and normal cells during 5-fluorouracil treatment was finally monitored.

Peroxynitrite ($ONOO^-$) is a highly reactive oxygen species (ROS) in living systems. It is formed by nitric oxide (NO) and $O_2^{\bullet -}$ in a diffusion-controlled manner (k = 0.4–1.9 × 10^{10} M^{-1} s^{-1}).[1] $ONOO^-$ plays key roles in maintaining the intracellular redox balance due to its strong oxidability. In addition, it always functions as a signaling molecule and exhibits antimicrobial and antibacterial activities.[2] In contrast, aberrant $ONOO^-$ expression *in vivo* is usually associated with cellular dysfunctions because it damages a wide variety of biomacromolecules like DNA and proteins,[3] resulting in diverse pathogenic effects, such as neurodegenerative, cardiovascular and inflammatory diseases, and cancers.[4] Therefore, it is important to develop reliable detection tools to monitor biological $ONOO^-$. However, efficient detection of intracellular $ONOO^-$ is challenging because it exhibits an extremely short half-life (<10 ms) and low steady-state concentration (nM range).[5] Over the past decade, fluorimetric analysis has been widely applied in the bioimaging of $ONOO^-$,[6] because of its superb sensitivity, high temporal and spatial resolution, and non-invasive imaging ability.[7]

To date, $ONOO^-$-specific fluorescent probes have been largely devised and used to monitor $ONOO^-$ fluctuations in various pathophysiological processes,[8–12] such as inflammation,[8] drug-induced organ toxicity,[9] ischemia reperfusion injury,[10] and diabetes.[11] These reports have led to a better understanding of the roles of $ONOO^-$ in certain biological courses. However, the development of $ONOO^-$ bioimaging is still hindered by the availability of fluorescent probes with excellent optical properties and scarce pathophysiological models. For example, most of the reported probes for $ONOO^-$ showed intensity changes at a single emission that are easily interfered with by a variety of analyte-independent factors, such as instrumental performance, the intracellular microenvironment around the probe molecule, the heterogeneous distribution of the probe, and photobleaching. Thus, ratiometric fluorescent probes that show optical changes at two emission bands and can avoid these interference sources for intensity-based probes are highly desired for $ONOO^-$ measurement.[13] In addition, some chemotherapeutic agents can kill cancer cells by augmenting intracellular oxidative stress, like 5-fluorouracil (5-FU), which yet lacks sufficient visual evidence.[14] Therefore, new ratiometric fluorescent probes are needed to monitor $ONOO^-$ fluctuation, to indirectly report oxidative stress during chemotherapy and for getting deeper insights into the therapeutic mechanism of drugs.

Here, we describe a series of phenothiazine-based fluorescent probes **3a**–**3c**. Phenothiazine was chosen as the fluorophore backbone because of its large Stokes shift and the reducibility of the sulfur atom.[15] The 2,3-diaminomaleonitrile was introduced into the 3-position of phenothiazine to construct a C=N bond that is susceptible to ROS.[16] It is variable at the 2-position of phenothiazine in these probes, and is supposed to affect their optical behaviors under oxidative stress. We demonstrated that 2-position non-substituted probe **3a** showed highly specific colorimetric and fluorescent changes toward $ONOO^-$ in a ratiometric manner, while **3b** and **3c** exhibited a similar response to $ONOO^-$ and ClO^-. Moreover, **3a** was capable of detecting exogenous and endogenous $ONOO^-$ in living cells. Finally, **3a** was utilized to visualize the generation of $ONOO^-$ in cancer cells and normal cells treated by 5-FU, a drug used in the treatment of various

[a] College of Chemistry and Chemical Engineering, Xinyang Normal University, Xinyang 464000, P. R. China. E-mail: houjiting2206@163.com, smallcoral@live.cn
[b] Ministry of Education, Key Laboratory of Hainan Trauma and Disaster Rescue, College of Emergency and Trauma, Hainan Medical University, Haikou 571199, China
[c] Phosphorus Chemical Engineering Research Center of Henan Province, College of Chemistry, Zhengzhou University, Zhengzhou 450001, P. R. China. E-mail: yeyong03@tsinghua.org.cn
[d] School of Chemistry and Materials Science, Hubei Engineering University, Xiaogan 432000, P. R. China

† Electronic supplementary information (ESI) available: Synthesis methods and supplementary figures. See DOI: 10.1039/c9cc09652c

Published on 28 January 2020. Downloaded by Universite Paris Descartes on 2/7/2020 3:20:41 AM.

cancers.[17] All of these probes were synthesized *via* a simple procedure and characterized by ^{1}H NMR, ^{13}C NMR, and HRMS (see ESI†).

We initially examined the optical response of probes **3a–3c** to reactive species, including ClO^-, H_2O_2, $ONOO^-$, $O_2^{\bullet-}$, ^{t}BuOOH, $^\bullet$OH, S^{2-}, and SO_3^{2-}. In PBS solution (pH 7.2–7.4, 10 mM, containing 1 mM Triton X-100), **3a**, **3b**, and **3c** displayed two main absorption bands at 435 nm and 347 nm, 454 nm and 343 nm, and 436 nm and 342 nm, respectively (Fig. S1 and S2, ESI†). Upon the addition of the analytes, the absorption of **3b** and **3c** obviously declined in the presence of $ONOO^-$ or ClO^-, while only $ONOO^-$ led to a loss of the absorption bands in **3a**. This also caused the generation of a new absorbance at 332 nm with a color change from light yellow to colorless, indicating that **3a** exhibited a higher selectivity toward $ONOO^-$ than the other two probes. A similar phenomenon was also observed in fluorescence tests. **3b** and **3c** emitted at 640 nm and 605 nm, respectively, while their fluorescence was largely quenched by $ONOO^-$ and ClO^-. To our delight, **3a** showed an emission band at 630 nm, which blue-shifted to 480 nm upon the addition of $ONOO^-$ with a 528-fold intensity ratio (I_{480}/I_{630}) enhancement (Fig. 1). A slight ratio change was also found in the presence of ClO^-, which is negligible when compared to that induced by $ONOO^-$. Other reactive species caused no fluorescence changes of **3a**. Since multiple heteroatoms are comprised in the structure of probe **3a**, we further checked its fluorescence response toward common metal ions, including Ca^{2+}, Cu^{2+}, Pb^{2+}, Zn^{2+}, and Ag^+ (Fig. S3, ESI†). No obvious spectral variations were recorded, demonstrating the high selectivity of **3a** toward $ONOO^-$. We note here that the slight modification at the 2-position of phenothiazine leads to distinguishing optical behaviors of the probes toward reactive species, which cannot be ignored for the design of phenothiazine-based probes.

The fluorescence response of **3a** toward $ONOO^-$ was further explored. The emission intensity of **3a** at 630 nm decreased with increasing concentrations of $ONOO^-$; a new emission band around 480 nm appeared, accompanied by a fluorescence color change from orange red to cyan (Fig. 2). The intensity ratio I_{480}/I_{630} reached a plateau when 11 equiv. $ONOO^-$ was added (Fig. S4, ESI†). A linear relationship between the intensity ratio and the concentrations of $ONOO^-$ was obtained from 0 to 2 μM (Fig. S5, ESI†) and the detection limit of **3a** toward

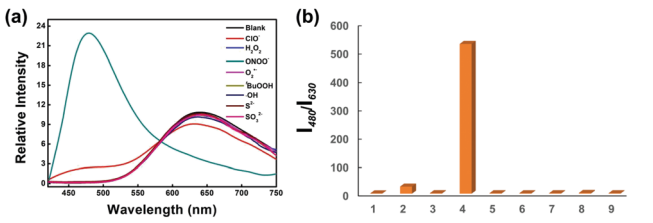

Fig. 1 (a) Emission spectra of **3a** (10 μM) before and after the addition of various reactive species (100 μM) in PBS solution (pH 7.2–7.4, 10 mM, containing 1 mM Triton X-100). λ_{ex} = 370 nm, slit width: 6 nm/6 nm. (b) The intensity ratio changes of **3a** before and after the addition of various reactive species. (1) Blank; (2) ClO^-; (3) H_2O_2; (4) $ONOO^-$; (5) $O_2^{\bullet-}$; (6) ^{t}BuOOH; (7) $^\bullet$OH; (8) S^{2-}; (9) SO_3^{2-}.

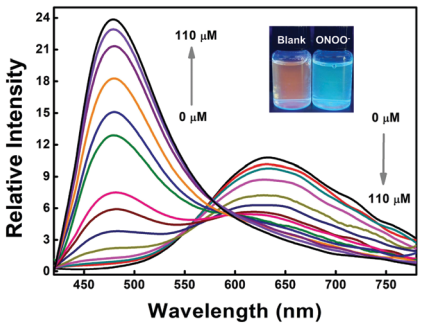

Fig. 2 Fluorescence titration of **3a** toward various concentrations of $ONOO^-$ in PBS solution (pH 7.2–7.4, 10 mM, containing 1 mM Triton X-100). λ_{ex} = 370 nm, slit width: 6 nm/6 nm. Inset: The photograph of **3a** before and after addition of $ONOO^-$ under 365 nm UV lamp.

$ONOO^-$ was calculated to be 19.4 nM signifying its high sensitivity. The fluorescence titration experiment of **3a** toward ClO^- was also performed to further verify its selectivity. Fig. S6 (ESI†) shows that at 14 equiv. of ClO^-, the intensity ratio change of **3a** was limited, again confirming the unique reaction between **3a** and $ONOO^-$.

Subsequently, the emission intensity ratio changes of **3a** in different pH buffered solutions were investigated (Fig. S7, ESI†). The intensity ratio I_{480}/I_{630} of **3a** was unchanged from pH 3 to 10. There was an obvious ratio enhancement upon the addition of $ONOO^-$ in the same pH range implying the ability of **3a** to measure analytes over a wide pH range, including physiological pH. In addition, the emission intensity of **3a** with or without $ONOO^-$ remained steady under continuous excitation for an hour (Fig. S8, ESI†), confirming their excellent photostability, which is an important feature for dynamic confocal bioimaging.

Time-dependent fluorescence emission changes in **3a** (10 μM) toward $ONOO^-$ (10 μM and 100 μM) were also exploited (Fig. S9, ESI†). The emission intensity of **3a** at 630 nm was sharply quenched in seconds when various amounts of $ONOO^-$ were added, indicating a rapid reaction between the probe and $ONOO^-$. Interestingly, when 100 μM $ONOO^-$ was added, the fluorescence at 480 nm was largely enhanced in the first few seconds, and then it gradually increased and almost reached a plateau in 9 min. In contrast, when 10 μM $ONOO^-$ was added, the emission of **3a** at 480 nm could plateau in 1 min. This out-of-step change at two emission bands of **3a** *versus* different amounts of $ONOO^-$ might be ascribed to the multi-step oxidation of the probe by $ONOO^-$.

To elucidate the reaction mechanism, a mixture of **3a** and $ONOO^-$ was extracted for MS analysis and ^{1}H NMR. As depicted in Fig. S10 and S11 (ESI†), apparent peaks at *m*/*z* 362.1057 and *m*/*z* 272.0720 were observed, corresponding to **3a-1** ([**3a-1** + H]$^+$: 362.1070) and **3a-2** ([**3a-2** + H]$^+$: 272.0740), respectively. A typical signal peak at 9.77 ppm in the ^{1}H NMR spectrum also supported the formation of the aldehyde product **3a-2** (Fig. S12, ESI†). Accordingly, a successive oxidation process of **3a** by $ONOO^-$ was proposed in Scheme 1b. The transformation of the sulfur atom to sulfoxide proceeded, rapidly leading to an immediate intensity decrease in **3a** at 630 nm and a synchronous partial fluorescence enhancement around 480 nm due to the inhibition of intramolecular charge transfer. The subsequent oxidative hydrolysis of the C=N bond of **3a-1** was slower, affording **3a-2** with a stronger fluorescence.

 This journal is © The Royal Society of Chemistry 2020

Published on 28 January 2020. Downloaded by Universite Paris Descartes on 2/7/2020 3:20:41 AM.

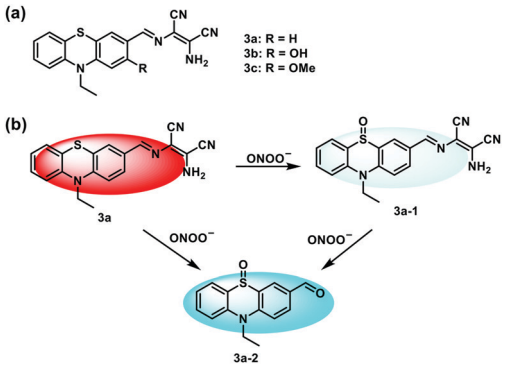

Scheme 1 (a) Structures of probes **3a–3c**; (b) the proposed reaction between **3a** and $ONOO^-$.

Therefore, a fast intensity enhancement at 480 nm in the first few seconds with a slower increment in the next few minutes was observed in the kinetics test (Fig. S9a, ESI†).

The desirable fluorescence properties of **3a** for $ONOO^-$ encouraged us to extend its utility to intracellular $ONOO^-$ detection. The cytotoxicity of **3a** in the human breast adenocarcinoma cell line (MCF-7 cells) was measured first. After incubation with various concentrations of **3a** for 24 h, more than 95% of the cells were found to be viable when 10 μM of the probe was added. More than 80% of the cells survived even when cultured with 30 μM of the probe, suggesting the outstanding biocompatibility of probe **3a** (Fig. S13, ESI†).

Next, the detection of exogenous and endogenous $ONOO^-$ in MCF-7 cells using **3a** was carried out. When cells were cultured with 10 μM of probe **3a** for 30 min, moderate red fluorescence and a weak cyan emission were observed. When 100 μM 3-morpholinosydnonimine (SIN-1, a $ONOO^-$ donor) was added for incubation for another 30 min, the red fluorescence nearly disappeared with apparent ratio changes (cyan/red) (Fig. S14, ESI†). The cells were further incubated with lipopolysaccharide (LPS) and interferon-γ (IFN-γ) for 24 h, and then incubated with **3a** for another 30 min. The fluorescence from the red channel diminished along with the emission enhancement from the cyan channel yielding an obvious ratio change in the overlay image (Fig. 3). The combined results showed that **3a** is nicely cell-permeable and can sensitively detect intracellular $ONOO^-$ in a ratiometric manner.

5-FU is a potent drug for the treatment of a variety of cancers by inhibiting DNA and RNA synthesis to drive cell death.[17] Recently, 5-FU-loaded nanoparticles have been reported to induce cell apoptosis in an ROS-dependent manner.[18] However, the augmented oxidative stress in cancer cells induced by 5-FU only has not been evidenced visually. As $ONOO^-$ is formed by $O_2^{\bullet -}$ and NO, it is regarded as an indirect indicator of oxidative stress. Thus, we used our probe to monitor $ONOO^-$ fluctuation to indirectly report oxidative stress in 5-FU-stimulated cancer cells, including MCF-7 cells and esophageal carcinoma cell line EC1 cells. MCF-7 cells and EC1 cells were treated with various concentrations of 5-FU (0 μM, 50 μM, 100 μM) for 20 h, respectively, followed by the culture with probe **3a**. As seen in Fig. 4 and Fig. S15 (ESI†), the emission from the red channel decreased when both cancer cells were treated with 50 μM of

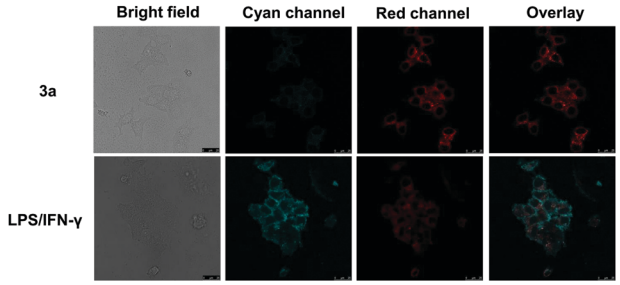

Fig. 3 Confocal fluorescence images of endogenous $ONOO^-$ in MCF-7 cells. (top) MCF-7 cells were stained with 10 μM **3a** for 30 min. (bottom) MCF-7 cells were incubated with LPS (1 μg mL^{-1}) and IFN-γ (50 ng mL^{-1}) for 24 h and then cultured with **3a** for another 30 min. Scale bar: 25 μm. Cyan channel: λ_{ex} = 405 nm, λ_{em} = 450–510 nm; red channel: λ_{ex} = 405 nm, λ_{em} = 610–670 nm.

5-FU, along with a simultaneous brightness increment in the cyan channel. The intensity ratio (cyan/red) obviously changed, suggesting that $ONOO^-$ was up-regulated in EC1 and MCF-7 cells treated by 5-FU and it might play a vital role in killing cancer cells. To the best of our knowledge, this is the first example of visualization of $ONOO^-$ generation in cancer cells during chemotherapy, which demonstrated the practicality of probe **3a**.

Moreover, $ONOO^-$ production in 5-FU treated-normal cells, human esophageal epithelial Het-1A cells was monitored to understand its drug safety. Unlike in cancer cells, the intensity ratio varied little in Het-1A cells incubated with 50 μM of 5-FU, indicating that the drug might show a weaker cytotoxicity to normal cells (Fig. S16, ESI†). However, evident changes in ratio color were visualized upon increment in the amount of 5-FU (100 and 200 μM), suggesting $ONOO^-$ up-regulation induced by the overdose of 5-FU in Het-1A cells. Hence, $ONOO^-$ can serve as a biomarker for assessing the safety of 5-FU in normal cells.

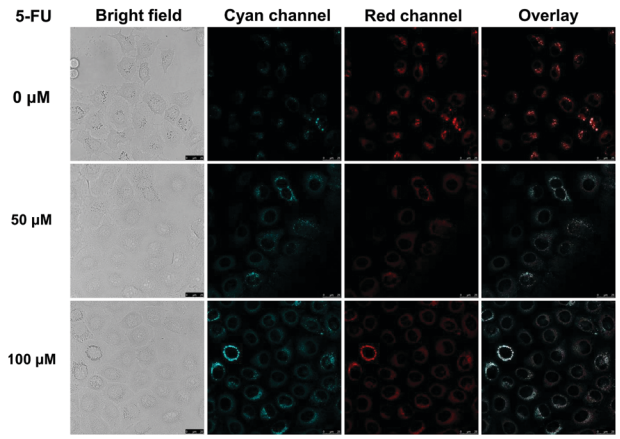

Fig. 4 Detection of $ONOO^-$ generation in 5-FU-treated EC1 cells. (a) EC1 cells were stained with different amounts of 5-FU (0 μM, 50 μM, 100 μM) for 20 h. Then, probe **3a** (10 μM) was added for incubation for another 30 min before confocal imaging. (b) Intensity ratio (cyan/red) changes *versus* different concentrations of 5-FU. Error bars are ± SEM. Scale bar: 25 μm. Cyan channel: λ_{ex} = 405 nm, λ_{em} = 450–510 nm; red channel: λ_{ex} = 405 nm, λ_{em} = 610–670 nm.

Published on 28 January 2020. Downloaded by Universite Paris Descartes on 2/7/2020 3:20:41 AM.

In summary, a series of phenothiazine-diaminomaleonitrile conjugates **3a–c** were presented, and **3a** without a substituent at the 2-position of the phenothiazine skeleton was verified to measure $ONOO^-$ in a ratiometric manner with excellent selectivity and high sensitivity. The multi-step oxidation of **3a** by $ONOO^-$ was postulated. Moreover, **3a** was confirmed to detect exogenous and endogenous $ONOO^-$ in living cells. Probe **3a** was used to image $ONOO^-$ up-regulation in 5-FU-treated cancer cells for the first time, including MCF-7 and EC1 cells. Meanwhile, the drug safety of 5-FU was preliminarily evaluated in Het-1A cells using probe **3a**. These results confirmed that probe **3a** holds value in monitoring $ONOO^-$ fluctuation during pathophysiological processes.

J.-T. H. acknowledges grants from the National Natural Science Foundation of China (no. 21807029), Key Laboratory of Emergency and Trauma (Hainan Medical University), and Ministry of Education (Grant KLET-201904); S. W. acknowledges grants from Nanhu Scholars Program for Young Scholars of XYNU. This research was also supported by the Analysis & Testing Center of Xinyang Normal University.

Conflicts of interest

There are no conflicts to declare.

Notes and references

1 C. Szabo, H. Ischiropoulos and R. Radi, *Nat. Rev. Drug Discovery*, 2007, **6**, 662–680.
2 L. Liaudet, G. Vassalli and P. Pacher, *Front. Biosci.*, 2009, **14**, 4809–4814.
3 (*a*) H. Kaur and B. Halliwell, *FEBS Lett.*, 1994, **350**, 9–12; (*b*) R. T. Dean, S. Fu, R. Stocker and M. J. Davies, *Biochem. J.*, 1997, **324**, 1–18.
4 (*a*) J. S. Beckman, M. Carson, C. D. Smith and W. H. Koppenol, *Nature*, 1993, **364**, 584–585; (*b*) H. Wiseman and B. Halliwell, *Biochem. J.*, 1996, **313**, 17–29; (*c*) S. M. Schieke, K. Briviba, L. O. Klotz and H. Sies, *FEBS Lett.*, 1999, **448**, 301–303; (*d*) W. Kossenjans, A. Eis, R. Sahay, D. Brochman and L. Myatt, *Am. J. Physiol. Heart Circ. Physiol.*, 2000, **278**, 1311–1319; (*e*) P. Pacher, J. S. Beckman and L. Liaudet, *Physiol. Rev.*, 2007, **87**, 315–424.
5 G. Ferrer-Sueta and R. Radi, *ACS Chem. Biol.*, 2009, **4**, 161–177.
6 (*a*) S. Wang, L. Chen, P. Jangili, A. Sharma, W. Li, J.-T. Hou, C. Qin, J. Yoon and J. S. Kim, *Coord. Chem. Rev.*, 2018, **374**, 36–54; (*b*) C. Prolo, N. Rios, L. Piacenza, M. N. Álvarez and R. Radi, *Free Radical Biol. Med.*, 2018, **128**, 59–68; (*c*) D. Lee, C. S. Lim, G. Ko, D. Kim, M. K. Cho, S.-J. Nam, H. M. Kim and J. Yoon, *Anal. Chem.*, 2018, **90**, 9347–9352; (*d*) J. Hou, K.-K. Yu, K. Sunwoo, W. Y. Kim, S. Koo, J. Wang, W. X. Ren, S. Wang, X.-Q. Yu and J. S. Kim, *Chem*, 2020, DOI: 10.1016/j.chempr.2019.12.005.
7 (*a*) D. W. Domaille, E. L. Que and C. J. Chang, *Nat. Chem. Biol.*, 2008, **4**, 168–175; (*b*) J.-T. Hou, W. X. Ren, K. Li, J. Seo, A. Sharma, X.-Q. Yu and J. S. Kim, *Chem. Soc. Rev.*, 2017, **46**, 2076–2090; (*c*) B. Zhang, X. Yang, R. Zhang, Y. Liu, X. Ren, M. Xian, Y. Ye and Y. Zhao, *Anal. Chem.*, 2017, **89**, 10384–10390; (*d*) M. Gao, F. Yu, C. Lv, J. Choo and L. Chen, *Chem. Soc. Rev.*, 2017, **46**, 2237–2271; (*e*) D. Wu, A. C. Sedgwick, T. Gunnlaugsson, E. U. Akkaya, J. Yoon and T. D. James, *Chem. Soc. Rev.*, 2017, **46**, 7105–7123; (*f*) J. Yan, S. Lee, A. Zhang and J. Yoon, *Chem. Soc. Rev.*, 2018, **47**, 6900–6916.
8 (*a*) Z. Song, D. Mao, S. H. P. Sung, R. T. K. Kwok, J. W. Y. Lam, D. Kong, D. Ding and B. Z. Tang, *Adv. Mater.*, 2016, **28**, 7249–7256; (*b*) Z. Li, S.-H. Yan, C. Chen, Z.-R. Geng, J.-Y. Chang, C.-X. Chen, B.-H. Huang and Z.-L. Wang, *Biosens. Bioelectron.*, 2017, **90**, 75–82; (*c*) D. Cheng, Y. Pan, L. Wang, Z. Zeng, L. Yuan, X. Zhang and Y.-T. Chang, *J. Am. Chem. Soc.*, 2017, **139**, 285–292.
9 (*a*) A. J. Shuhendler, K. Pu, L. Cui, J. P. Uetrecht and J. Rao, *Nat. Biotechnol.*, 2014, **32**, 373–382; (*b*) J. Peng, A. Samanta, X. Zeng, S. Han, L. Wang, D. Su, D. T. B. Loong, N.-Y. Kang, S.-J. Park, A. H. All, W. Jiang, L. Yuan, X. Liu and Y.-T. Chang, *Angew. Chem., Int. Ed.*, 2017, **56**, 4165–4169; (*c*) Y. Li, X. Xie, X. Yang, M. Li, X. Jiao, Y. Sun, X. Wang and B. Tang, *Chem. Sci.*, 2017, **8**, 4006–4011; (*d*) X. Xie, F. Tang, G. Liu, Y. Li, X. Su, X. Jiao, X. Wang and B. Tang, *Anal. Chem.*, 2018, **90**, 11629–11635; (*e*) D. Cheng, J. Peng, Y. Lv, D. Su, D. Liu, M. Chen, L. Yuan and X. Zhang, *J. Am. Chem. Soc.*, 2019, **141**, 6352–6361; (*f*) W.-L. Jiang, Y. Li, W.-X. Wang, Y.-T. Zhao, J. Fei and C.-Y. Li, *Chem. Commun.*, 2019, **55**, 14307–14310.
10 (*a*) T. Peng, X. Chen, L. Gao, T. Zhang, W. Wang, J. Shen and Dan Yang, *Chem. Sci.*, 2016, **7**, 5407–5413; (*b*) W. Zhang, J. Liu, P. Li, X. Wang, S. Bi, J. Zhang, W. Zhang, H. Wang and B. Tang, *Biomaterials*, 2019, **225**, 119499.
11 (*a*) J. Miao, Y. Huo, Q. Liu, Z. Li, H. Shi, Y. Shi and W. Guo, *Biomaterials*, 2016, **107**, 33–43; (*b*) J. Miao, Y. Huo, H. Shi, J. Fang, J. Wang and W. Guo, *J. Mater. Chem. B*, 2018, **6**, 4466–4473.
12 (*a*) T. Peng, N.-K. Wong, X. Chen, Y.-K. Chan, D. H.-H. Ho, Z. Sun, J. J. Hu, J. Shen, H. El-Nezami and D. Yang, *J. Am. Chem. Soc.*, 2014, **136**, 11728–11734; (*b*) X. Li, R. R. Tao, L. J. Hong, J. Cheng, Q. Jiang, Y. M. Lu, M. H. Lao, W. F. Ye, N. N. Lu, F. Han, Y. Z. Hu and Y. H. Hu, *J. Am. Chem. Soc.*, 2015, **137**, 12296–12303; (*c*) S. Palanisamy, P. Y. Wu, S. C. Wu, Y. J. Chen, S. C. Tzou, C. H. Wang, C. Y. Chen and Y. M. Wang, *Biosens. Bioelectron.*, 2017, **91**, 849–856; (*d*) J. Li, C. S. Lim, G. Kim, H. M. Kim and J. Yoon, *Anal. Chem.*, 2017, **89**, 8496–8500; (*e*) X. Xie, G. Liu, X. Su, Y. Li, Y. Liu, X. Jiao, X. Wang and B. Tang, *Anal. Chem.*, 2019, **91**, 6872–6879.
13 M. H. Lee, J. S. Kim and J. L. Sessler, *Chem. Soc. Rev.*, 2015, **44**, 4185–4191.
14 P. T. Schumacker, *Cancer Cell*, 2006, **10**, 175–176.
15 (*a*) F. Liu, T. Wu, J. Cao, H. Zhang, M. Hu, S. Sun, F. Song, J. Fan, J. Wang and X. Peng, *Analyst*, 2013, **138**, 775–778; (*b*) H. Xiao, K. Xin, H. Dou, G. Yin, Y. Quan and R. Wang, *Chem. Commun.*, 2015, **51**, 1442–1445; (*c*) F. Liu, J. Du, D. Song, M. Xu and G. Sun, *Chem. Commun.*, 2016, **52**, 4636–4639.
16 (*a*) L. Yuan, W. Lin, J. Song and Y. Yang, *Chem. Commun.*, 2011, **47**, 12691–12693; (*b*) J.-T. Hou, H. S. Kim, C. Duan, M. S. Ji, S. Wang, L. Zeng, W. X. Ren and J. S. Kim, *Chem. Commun.*, 2019, **55**, 2533–2536.
17 J. Boyer, P. J. Maxwell, D. B. Longley and P. G. Johnston, *Anticancer Res.*, 2004, **24**, 417–423.
18 (*a*) W. Liu, X. Li, Y. S. Wong, W. Zheng, Y. Zhang, W. Cao and T. Chen, *ACS Nano*, 2012, **6**, 6578–6591; (*b*) I. Matai, A. Sachdev and P. Gopinath, *Biomater. Sci.*, 2015, **3**, 457–468.

 This journal is © The Royal Society of Chemistry 2020